

# Tuneable Dielectric Properties Derived from Nitrogen-Doped Carbon Nanotubes in PVDF-Based Nanocomposites

Shital Patangrao Pawar,<sup>†,⊥</sup> Mohammad Arjmand,<sup>‡,⊥</sup> Petra Pötschke,<sup>§</sup> Beate Krause,<sup>§</sup> Dieter Fischer,<sup>§</sup> Suryasarathi Bose,<sup>\*,||</sup> and Uttandaraman Sundararaj<sup>\*,†</sup>

<sup>†</sup>Department of Chemical and Petroleum Engineering, University of Calgary, Calgary, AB, Canada T2N 1N4

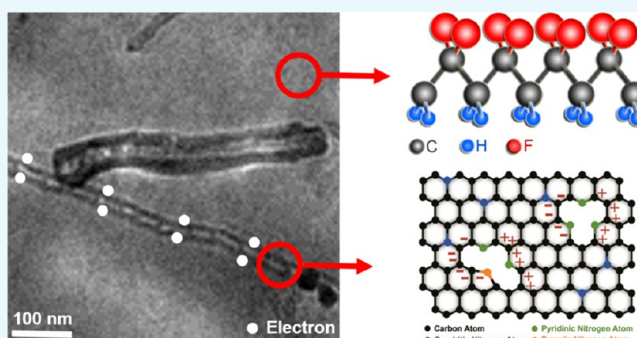
<sup>‡</sup>School of Engineering, University of British Columbia, Kelowna, BC, Canada V1V 1V7

<sup>§</sup>Leibniz Institute of Polymer Research Dresden (IPF), Hohe Str. 6, 01069 Dresden, Germany

<sup>||</sup>Department of Materials Engineering, Indian Institute of Science, Bangalore 560012, India

## Supporting Information

**ABSTRACT:** Nitrogen-doped multiwall carbon nanotubes (N-MWNTs) with different structures were synthesized by employing chemical vapor deposition and changing the argon/ethane/nitrogen gas precursor ratio and synthesis time, and broadband dielectric properties of their poly(vinylidene fluoride) (PVDF)-based nanocomposites were investigated. The structure, morphology, and electrical conductivity of synthesized N-MWNTs were assessed via Raman spectroscopy, scanning electron microscopy, transmission electron microscopy, thermogravimetric analysis (TGA), X-ray photoelectron spectroscopy, and powder conductivity techniques. The melt compounded PVDF nanocomposites manifested significantly high real part of the permittivity ( $\epsilon'$ ) along with low dissipation factor ( $\tan \delta_\epsilon$ ) in 0.1 kHz to 1 MHz frequency range, suggesting use as efficient charge-storage materials. Longer synthesis time resulted in enhanced carbon purity as well as higher thermal stability, determined via TGA analysis. The inherent electrical conductivity of N-MWNTs scaled with the carbon purity. The charge-storage ability of the developed PVDF nanocomposites was commensurate with the amount of the nitrogen heteroatom (i.e., self-polarization), carbon purity, and inherent electrical conductivity of N-MWNTs and increased with better dispersion of N-MWNTs in PVDF.



## 1. INTRODUCTION

Multifunctional polymer-based nanocomposites containing conducting carbonaceous nanofillers have gained a great deal of interest as charge-storage materials.<sup>1–3</sup> Materials possessing a high real permittivity ( $\epsilon'$ ) coupled with a low dissipation factor ( $\tan \delta_\epsilon$ ) measured over broadband frequency range are highly desired in modern electronics and communication sectors. In this context, poly(vinylidene fluoride) (PVDF) and its co-polymers have attracted significant research interest, due to their large dielectric constant versus other conventional polymers.<sup>4,5</sup>

PVDF offers various advantages, such as flexibility, easy processability, and lightweight, compared to the traditional charge-storing ceramics. Nevertheless, the inferior inherent dielectric constant of PVDF over ceramics limits its widespread applications. Hence, in the context of charge-storing ability, it is important to enhance the dielectric constant of the polymer alongside with retaining a small dielectric loss. In this framework, polymer nanocomposites containing carbonaceous nanofillers, such as carbon nanotubes (CNTs) and graphene sheets, have shown interesting outcomes toward enhancing the

dielectric constant of the system and surmounting the issues related to traditional ceramic materials.<sup>6,7</sup>

Over the years, the chemical and structural modifications of functional fillers have become an effective way to tailor the inherent properties of these fillers to use them for the charge-storage applications.<sup>7–9</sup> In this context, the unique technique of nitrogen doping of CNTs was employed to incorporate polarizing centers (i.e., self-polarization) within CNTs, facilitating large real permittivity.<sup>5,10–13</sup> In fact, enhanced real permittivity derived from nitrogen-doped multiwall carbon nanotubes (N-MWNTs) in polymer-based nanocomposites can be effectively used for charge-storage applications.

In this work, nitrogen doping was employed as a tool to tune the dielectric performance of chemical vapor deposition (CVD)-grown multiwall carbon nanotubes (MWNTs), and therefrom prepared PVDF-based nanocomposites. In the case of CVD method, there is no need of patterned substrate for

Received: June 5, 2018

Accepted: August 14, 2018

Published: August 27, 2018

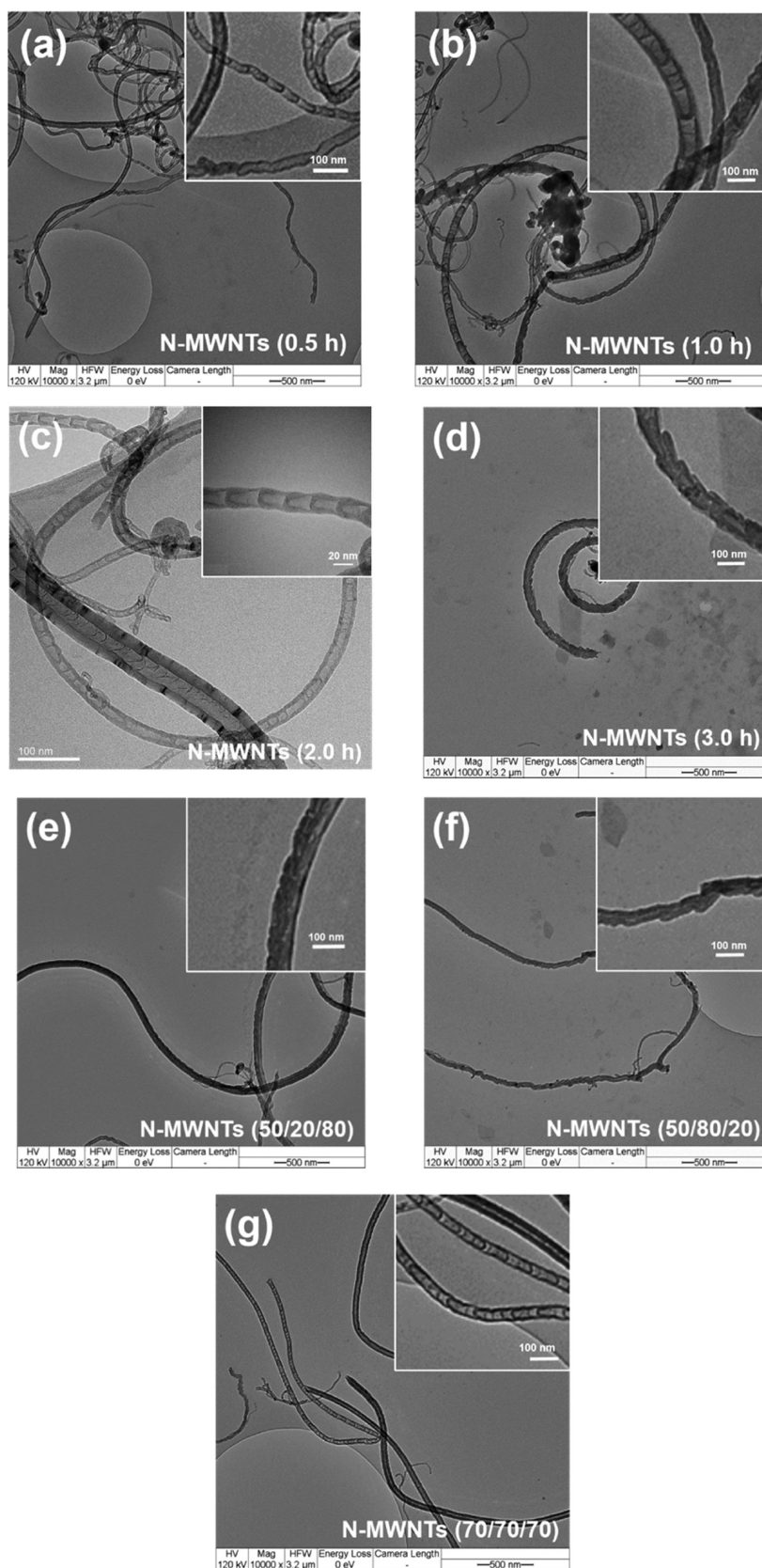


**Figure 1.** TEM micrographs of N-MWNTs synthesized at gas ratio of 50:50:50 at different synthesis time (a) 0.5 h, (b) 1.0 h, (c) 2.0 h, and (d) 3.0 h; and at synthesis time of 2.0 h at different gas ratios (e) 50:20:80, (f) 50:80:20, and (g) 70:70:70. TEM micrograph of N-MWNTs synthesized at gas ratio of 50:50:50 and 2.0 h synthesis time is presented in (c). High-magnification micrographs are shown as inset.

CNT growth. Moreover, this method provides a large degree of freedom in developing structural and functional properties

of CNTs. The effects of synthesis temperature and type of catalyst used to grow nitrogen-doped MWNTs on structural

properties of N-MWNTs have been reported in the literature.<sup>5,11,13</sup> On the other hand, the effect of synthesis time, which governs the growth of MWNTs, and precursors' gas ratio (i.e., the source of carbon and nitrogen), which defines the carbon purity and amount of polarizing centers, on the functional properties of N-MWNTs remained unexplored. Therefore, to gain a complete understanding of N-MWNTs synthesis parameters and their effect on structural and electrical properties of N-MWNTs, various influential parameters, such as carbon purity, structural defects, amount of nitrogen content, and inherent electrical conductivity of N-MWNTs, were varied by altering the CNT synthesis time and the precursors' gas ratio. Thereafter, the effects of these parameters on the broadband dielectric properties of PVDF/N-MWNTs nanocomposites were explored. Accordingly, this study builds strong ground about the interplay between N-MWNTs synthesis condition, N-MWNTs structure, and resulting broadband dielectric properties of the nanocomposites thereof.

## 2. RESULTS AND DISCUSSION

**2.1. Properties of N-MWNTs.** **2.1.1. Morphology by Transmission Electron Microscopy (TEM).** The overall morphology, graphitic wall structure, and aspect ratio of CNTs play vital roles on the intrinsic electrical properties of CNTs as well as the properties of their polymer-based nanocomposites. It is well known that the conductive network formation of CNTs in a given polymer matrix is greatly controlled by the aspect ratio and the electronic structure of the CNTs.<sup>14,15</sup> Therefore, overall morphology, graphitic wall structure, length, and diameter of the synthesized N-MWNTs were assessed using TEM analysis. Figure 1 shows representative TEM micrographs of N-MWNTs synthesized at different synthesis time and gas ratios. On the basis of the TEM analysis, N-MWNTs synthesized at various synthesis time and gas ratios revealed a bamboo-like structure along with a closed cap assembly (see insets of Figure 1a–g). It can be noticed that during N-MWNTs growth, the outer wall of N-MWNTs grew straight; however, inner walls significantly distorted inward, eventually leading to closed channels. This further results in uneven wall thickness and decreased crystallinity of the graphitic structure.

The bamboo-like structure of N-MWNTs is widely reported in the literature and has been ascribed to the substitution of the nitrogen atoms in the graphitic structure of MWNTs.<sup>16–20</sup> However, it is assumed that this unique structure is not only governed by the substituted nitrogen atom, but also controlled by the catalyst and nitrogen source used to grow N-MWNTs.<sup>5,21–24</sup>

The length distribution and average diameter of N-MWNTs were studied using TEM, and are listed in Table 1. The effect of synthesis time on the length of N-MWNTs is very evident from the TEM analysis, where N-MWNTs synthesized at 0.5 h depicted longest N-MWNTs over 1.0, 2.0, and 3.0 h along with a broad length distribution. Previously, it has been shown that the incorporation of nitrogen in the structure of MWNTs significantly reduces the length,<sup>5,23</sup> mainly due to the bamboo-like structure of N-MWNTs, where a reduced amount of carbon takes part in the axial growth of N-MWNTs. From the XPS analysis (discussed later), a direct relationship between the nitrogen content and the synthesis time was observed. Hence, higher content of nitrogen in N-MWNTs structure led to a more distorted structure along with a limited axial growth.

**Table 1. Typical Values of Length Distribution and Mean Diameters for N-MWNTs Synthesized by Varying Synthesis Time and Gas Ratios (Argon/Ethane/Nitrogen), Obtained from TEM Analysis**

N-MWNTs		length distribution values			average diameter (nm)
synthesis time (h)	gas ratio (sccm)	$x_{10}$ (nm)	$x_{50}$ (nm)	$x_{90}$ (nm)	
0.5	50:50:50	355	1064	4984	33 ± 12
1.0	50:50:50	289	851	2423	29 ± 12
2.0	50:50:50	216	907	3838	35 ± 15
3.0	50:50:50	282	799	3599	38 ± 14
2.0	50:20:80	317	861	2887	39 ± 14
2.0	50:50:50	216	907	3838	35 ± 15
2.0	50:80:20	323	1312	7401	39 ± 13
2.0	70:70:70	352	1458	5930	36 ± 12

This could justify lower length of N-MWNTs synthesized at 1.0 h. Moreover, large variations in the diameters of the synthesized N-MWNTs were observed (Table 1). The diameter of N-MWNTs was slightly higher at the longest synthesis time (i.e., 2.0 and 3.0 h). Since the diameter of MWNTs linearly varies with the size of the catalyst, increased diameter of N-MWNTs in this case is attributed to the sintering of catalyst particles at the longer synthesis time.

Considering the effect of the gas ratio on N-MWNTs length and diameter (Table 1), a very broad length distribution was observed. The longest N-MWNTs were synthesized at the gas ratio of 50:80:20, followed by 70:70:70, 50:50:50, and 50:20:80. Interestingly, the length of N-MWNTs scaled with the amount of ethane (i.e., source of carbon) feed. Moreover, the role of nitrogen in barricading the growth of N-MWNTs should be taken into account. In case of N-MWNTs synthesized at the gas ratio of 50:80:20, the longest N-MWNTs were due to maximum ethane feed coupled with the lowest amount of nitrogen. Therefore, it can be concluded that the feed of ethane and presence of nitrogen in the structure mainly control the length of N-MWNTs. Moreover, from the TGA analysis (shown later), it was observed that N-MWNTs with higher crystallinity are also longer. At the investigated synthesis temperature and time, no significant effect of gas ratio on the diameter of N-MWNTs was observed.

**2.1.2. Morphology by Scanning Electron Microscopy (SEM).** Further evidence of the overall morphology of N-MWNTs was found via SEM micrographs (Figure 2). The images reveal again that there is a broad diameter distribution for all N-MWNT samples, which agrees with the TEM analysis (Table 1). In the case of N-MWNTs synthesized for 0.5 h, though the number of substrate particles was fixed while synthesis, number of N-MWNTs was significantly small and increased further at longer synthesis time (i.e., 1.0, 2.0, and 3.0 h). Higher amount of catalyst resulted in lower carbon purity, which will later be verified with TGA. Similarly, the effect of gas ratio on the purity of N-MWNTs was well evident. Small chunks of substrate particles were observed in the case of N-MWNTs synthesized at the gas ratio of 50:20:80, which are evident from the inset of Figure 2e. The SEM micrographs of N-MWNTs synthesized at the gas ratios of 50:80:20, 50:50:50, and 70:70:70 show no significant presence of such substrate particles. These observations will be later verified with TGA.

**2.1.3. Nitrogen Content by X-ray Photoelectron Spectroscopy (XPS).** The quantitative analysis of nitrogen present in N-MWNTs was performed using X-ray photoelectron spectroscopy.

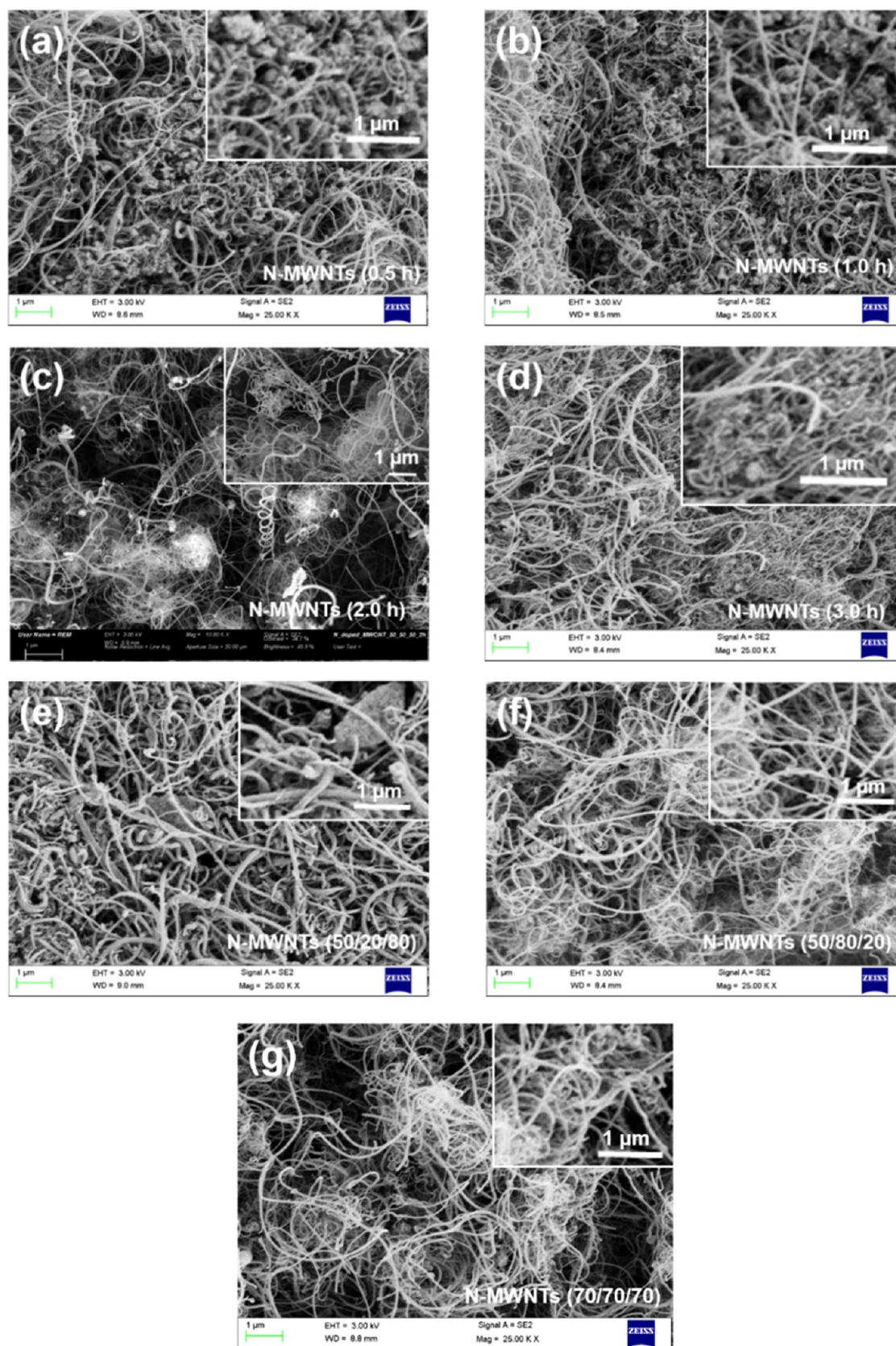


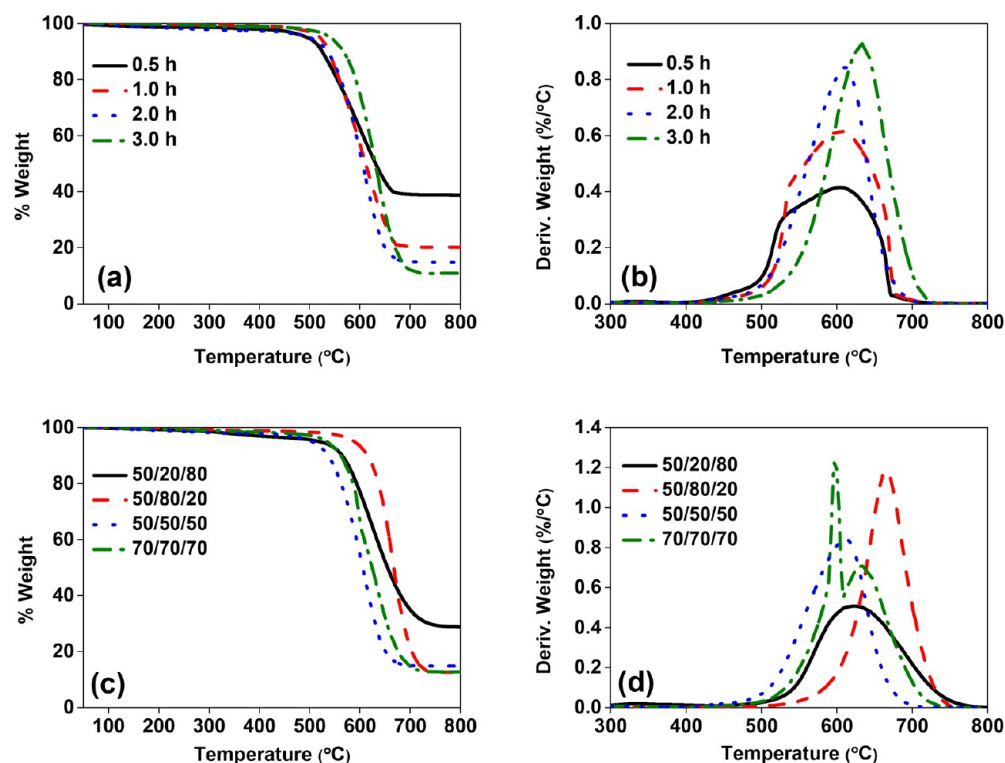
**Figure 2.** SEM micrographs of N-MWNTs synthesized at gas ratio of 50:50:50 at different synthesis time (a) 0.5 h, (b) 1.0 h, (c) 2.0 h, and (d) 3.0 h; and at synthesis time of 2.0 h at different gas ratios (e) 50:20:80, (f) 50:80:20, and (g) 70:70:70. High-magnification micrographs are shown in the inset.

**Table 2.** Concentration of Nitrogen Present in N-MWNTs, Synthesized by Varying Synthesis Time and Gas Ratios (Argon/Ethane/Nitrogen), Obtained from XPS Analysis

N-MWNTs	synthesis time (h)				gas ratio (sccm)			
	0.5	1.0	2.0	3.0	50:20:80	50:80:20	50:50:50	70:70:70
nitrogen content (atom %)	0.35	0.45	0.88	0.56	0.58	0.41	0.88	0.66

**Table 3.**  $I_D/I_G$  for N-MWNTs Synthesized by Varying Synthesis Time and Gas Ratio (Argon/Ethane/Nitrogen)

N-MWNT	synthesis time (h)				gas ratio (sccm)			
	0.5	1.0	2.0	3.0	50:20:80	50:80:20	50:50:50	70:70:70
$I_D/I_G$	$0.67 \pm 0.15$	$0.8 \pm 0.34$	$0.94 \pm 0.14$	$0.76 \pm 0.41$	$0.65 \pm 0.49$	$0.98 \pm 0.24$	$0.94 \pm 0.14$	$0.86 \pm 0.09$

**Figure 3.** TGA thermograms of N-MWNTs synthesized at different (a, b) synthesis time and (c, d) gas ratios.

copy (XPS). The XPS wide scan spectra for N-MWNTs synthesized at different synthesis time and gas ratios are shown in Figures S1 and S2, respectively. The effect of synthesis time on nitrogen doping is evident from the XPS results, which show that the nitrogen content is significantly enhanced by increasing the synthesis time (Table 2). This might be attributed to the decomposition of a higher amount of ammonia (i.e., a source of nitrogen) and larger substitution of nitrogen atoms in the graphitic structure of N-MWNTs with increasing synthesis time at a given synthesis temperature. However, highest incorporation of nitrogen in N-MWNTs was observed at 2.0 h, and further decreased at 3.0 h. The presence of nitrogen greatly affects the structural stability as well as the morphology of N-MWNTs, which was also evident from the TEM analysis (insets of Figure 1a–g). It is also well established that the presence of nitrogen in the MWNT structure leads to shorter MWNTs as compared to MWNTs grown from pure carbon.<sup>25,26</sup> In addition, it was observed that the gas feed ratio greatly influences the nitrogen content in N-MWNTs. For instance, the highest nitrogen content (i.e., 0.88 atom %) was observed in N-MWNTs synthesized at the gas

ratio of 50:50:50. In case of 50:20:80, though the amount of ammonia fed was higher over 50:50:50, the nitrogen content was significantly less. In this case, the incorporation of nitrogen was limited by the small amount of ethane (i.e., 20 sccm) available for N-MWNT growth.

**2.1.4. Defect Content by Raman Spectroscopy.** As per previous studies, it is well known that nitrogen doping leads to the generation of defect sites in the graphitic structure of CNTs.<sup>27–29</sup> The incorporation of nitrogen in CNT structures leads to different types of defects, such as pentagons, heptagons, and substitution of the nitrogen atom in carbon hexagons.<sup>5,11</sup> The above-mentioned defects substantially alter the electronic properties of N-MWNTs. Moreover, the generated defects could act as polarizing centers and influence the dielectric properties of N-MWNTs.<sup>10,12</sup>

The effect of nitrogen doping on the structural properties of N-MWNTs was studied using Raman spectroscopy. The Raman spectra for N-MWNTs synthesized at different synthesis time and gas ratios are shown in Figure S3. To understand the defects present in N-MWNTs, the intensity ratios of D-band and G-band (i.e.,  $I_D/I_G$ ) were estimated, and

**Table 4. TGA Results of N-MWNTs Synthesized at Different Synthesis Time and Gas Ratios**

synthesis parameters	synthesis time (h)				gas ratio (sccm)			
	0.5	1.0	2.0	3.0	50:20:80	50:80:20	50:50:50	70:70:70
N-MWNT								
carbon purity (%)	61.2	79.8	85.1	85.2	71.1	86.4	85.1	87
inflection point (°C)	603	603	605	633	622	664	605	598

given in Table 3. Considering different synthesis time, the N-MWNTs synthesized at 2.0 h show the most defective structure, with an  $I_D/I_G$  of  $0.94 \pm 0.14$ , followed by 1.0, 3.0, and 0.5 h. The effect of gas ratio on defects was apparent from  $I_D/I_G$ . The lowest amount of defects was observed for N-MWNTs synthesized at a gas ratio of 50:20:80 with an  $I_D/I_G$  of  $0.65 \pm 0.49$ , followed by 70:70:70, 50:50:50, and 50:80:20. The highest  $I_D/I_G$  of  $0.98 \pm 0.24$  observed for N-MWNTs synthesized with gas ratio of 50:80:20 suggests highly distorted structure. The  $I_D/I_G$  was expected to be in line with the amount of nitrogen present; however, no direct relationship between  $I_D/I_G$  and nitrogen content was observed for either synthesis time or gas ratio. Given the Raman spectroscopy and XPS analysis, it may be concluded that other factors than nitrogen content, such as impurities, affect the Raman spectra.

**2.1.5. Thermal Stability and Carbon Purity by Thermogravimetric Analysis (TGA).** The thermal stability and carbon purity of N-MWNTs were assessed using thermogravimetric analysis (TGA). All TGA experiments were performed in air atmosphere, and residual mass observed after degradation of N-MWNTs was assigned to the alumina substrate and metal oxide catalyst particles (Figure 3).

The inflection points for N-MWNTs synthesized at 0.5, 1.0, 2.0, and 3.0 h were recorded at 603, 603, 605, and 633 °C, respectively (Table 4). Significantly higher thermal stability of N-MWNTs synthesized at 3.0 h over 0.5, 1.0, and 2.0 h suggests higher crystallinity for 3.0 h. Since carbon purity is inversely proportional to residual mass,<sup>13</sup> it can be concluded that the carbon purity scales with the synthesis time. For instance, N-MWNTs synthesized at 3.0 h depicted carbon purity of 85.2%, suggesting relatively higher purity. This is attributed to enhanced gas precursor decomposition at increased synthesis time, leading to higher carbon purity.

The gas ratio also depicted a significant effect on the thermal stability and carbon purity. N-MWNTs synthesized at the gas ratio of 50:80:20 show the highest thermal stability and optimum carbon purity, suggesting the synthesis of highly crystalline N-MWNTs. Interestingly, N-MWNTs synthesized at the gas ratio of 70:70:70 depicted two degradation peaks, suggesting, at this gas ratio, two different types of N-MWNTs were synthesized (Figure 3d). The poor thermal stability in case of N-MWNTs synthesized at the gas ratio of 70:70:70 over 50:80:20 was ascribed to the amorphous carbon and distorted structure, due to the presence of the higher amount of nitrogen, as inferred from the XPS analysis. It was expected that the less defective N-MWNTs result in higher crystallinity;<sup>30</sup> however, in this case, amount of defects and crystallinity observed from thermal stability was not in line. This suggests that apart from defective structure, various other parameters also control the crystallinity of the N-MWNTs.

It is important to note that the iron catalyst substrate particles are electrically insulative in nature and have a significantly smaller surface area than N-MWNTs. The catalyst surface area also decreases further at high synthesis temperatures due to the sintering process. Therefore, the presence of substrate and catalyst leads to a decreased effective bulk

electrical conductivity of N-MWNTs. Hence, N-MWNTs with high carbon purity are necessary for electrical conductivity as well as for charge-storage applications.

**2.1.6. N-MWNT Powder Conductivity.** The inherent electrical conductivity of N-MWNTs plays a vital role in defining the electrical conductivity and charge-storage ability of their nanocomposites. The electrical properties of N-MWNTs are governed by various parameters, such as graphitic structure, defects, and carbon purity. To get a rough estimate of the inherent electrical conductivity of N-MWNTs, direct current (DC) electrical conductivity of compressed N-MWNT powders at different applied pressures was measured (Table 5). The electrical powder conductivity was found to scale with

**Table 5. Electrical Powder Conductivity at Varied Pressures of N-MWNTs Synthesized at Different Synthesis Time and Gas Ratios**

N-MWNTs	electrical powder conductivity (S/cm)				
	5 MPa	10 MPa	20 MPa	25 MPa	30 MPa
synthesis time (0.5 h)	8.5	10.9	14.7	17.0	17.7
synthesis time (1.0 h)	7.6	11.6	14.8	19.1	20.0
synthesis time (2.0 h)	8.9	12.9	17.0	19.8	20.6
synthesis time (3.0 h)	10.4	14.0	18.8	22.9	24.5
gas ratio (50:20:80)	9.2	11.7	14.8	18.6	20.0
gas ratio (50:80:20)	9.3	13.1	17.2	20.0	20.9
gas ratio (50:50:50)	8.9	12.9	17.0	19.8	20.6
gas ratio (70:70:70)	9.6	13.1	17.4	19.9	22.4

synthesis time. This is mainly ascribed to the higher carbon purity of N-MWNTs synthesized at longer synthesis time, as obtained from TGA results. On the other hand, the nitrogen content was also observed to increase at longer synthesis time. The nitrogen present in N-MWNTs structure acts as scattering points against nomadic charges, and thus decreases the current flow in N-MWNTs.

The gas ratio used for the synthesis of N-MWNTs showed no significant effect on the powder conductivity of N-MWNTs (Table 5). Slightly enhanced electrical powder conductivity is observed for N-MWNTs synthesized at the gas ratio of 70:70:70 (i.e., 22.4 S/cm at 30 MPa) over the gas ratio of 50:20:80 (i.e., 20 S/cm at 30 MPa), 50:50:50 (i.e., 20.6 S/cm at 30 MPa), and 50:80:20 (i.e., 20.9 S/cm at 30 MPa). The N-MWNTs synthesized at the gas ratio of 50:20:80 depicted lowest powder conductivity despite having less defective structure. This was mainly due to minimum carbon purity of N-MWNTs synthesized at 50:20:80. The N-MWNTs with high intrinsic conductivity are expected to provide larger current flow in PVDF nanocomposites via interconnected network of N-MWNTs.

**2.2. Structure and Properties of PVDF-Based Melt-Mixed Nanocomposites.** **2.2.1. Dispersion of N-MWNTs in PVDF at Various Length Scales.** The electrical properties of polymer-based nanocomposites are governed not only by the inherent properties of the conducting filler, but also greatly controlled by its dispersion state in a given matrix.<sup>31,32</sup> An

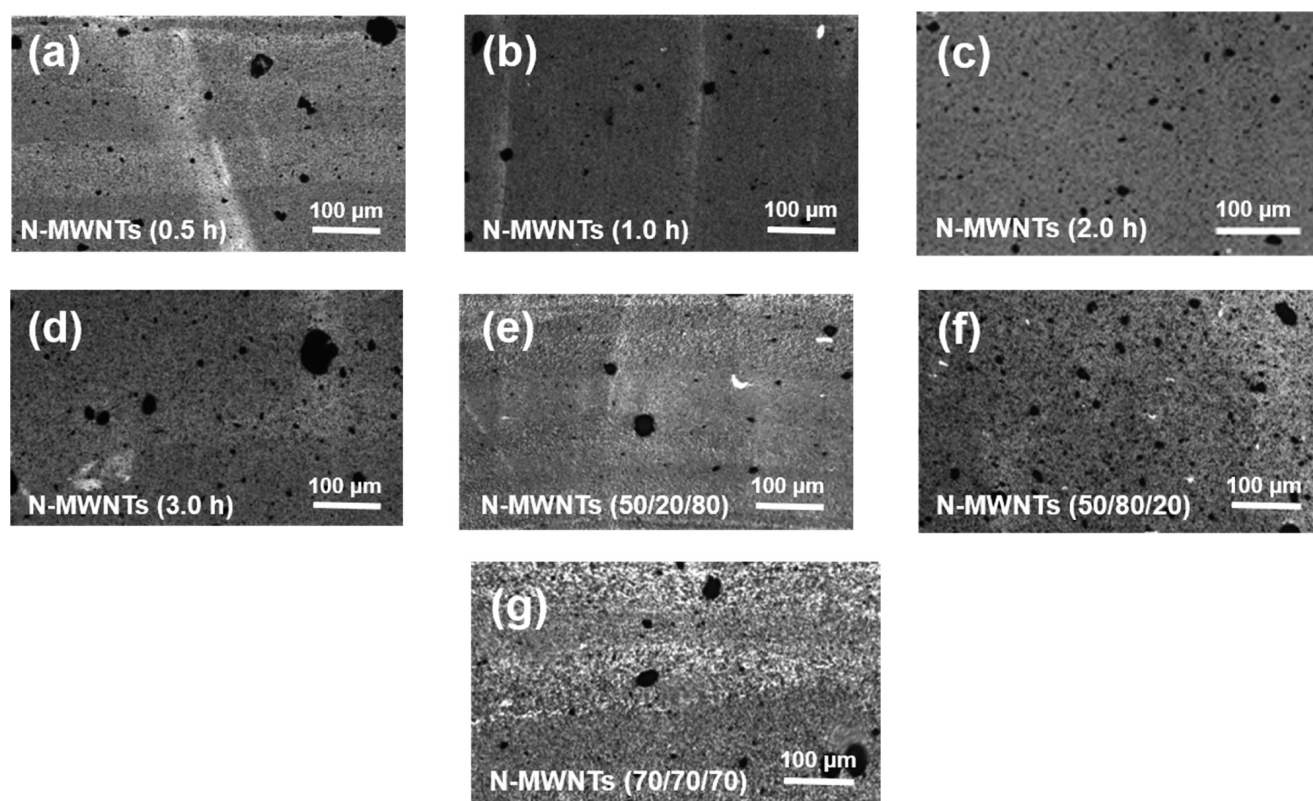


**Figure 4.** Optical micrographs of PVDF nanocomposites containing 2.0 wt % of N-MWNTs synthesized at gas ratio of 50:50:50 at different synthesis time (a) 0.5 h, (b) 1.0 h, (c) 2.0 h, and (d) 3.0 h; and at synthesis time of 2.0 h at different gas ratios (e) 50:20:80, (f) 50:80:20, and (g) 70:70:70. Optical micrographs of PVDF nanocomposites containing 2.0 wt % of N-MWNTs synthesized at gas ratio of 50:50:50 and 2.0 h synthesis time is presented in (c).

effective dispersion of N-MWNTs in the PVDF matrix is necessary to take advantage of the excellent properties of the functional N-MWNTs in the nanocomposite. The required conducting filler network should be achieved at low filler loadings, implying that most of the primary nanotube agglomerates are dispersed into individualized nanotubes while retaining their initial length. Therefore, we made an attempt to investigate the state of nanotube dispersion of N-MWNTs in the PVDF matrix at three different length scales.

First, the microdispersion of N-MWNTs in the PVDF matrix and the existence of remaining primary agglomerates were assessed using optical micrographs, and quantitative analysis was performed by estimating the agglomerate area ratio. Figure 4 shows representative optical micrographs of PVDF nanocomposites containing 2 wt % N-MWNTs. The effect of synthesis time on the dispersion state of N-MWNTs in the PVDF matrix is very evident; the nanocomposite containing N-MWNTs synthesized at 3.0 h shows the highest amount of agglomerates and the largest agglomerates in the PVDF matrix, followed by N-MWNTs synthesized at 2.0, 0.5, and 1.0 h (see Table 6). The PVDF nanocomposites containing N-MWNTs synthesized at 1.0 h depicted the best dispersion of N-MWNTs with an agglomerate area ratio of only  $1.02 \pm 0.35\%$ .

In a method described first by Arjmand and Sundararaj,<sup>26</sup> film transparency was used to analyze the dispersion state of N-MWCNTs in PVDF and in this method, the amount of smaller agglomerates with sizes equal to or slightly larger than the wavelength of visible light (i.e., 400–700 nm) was determined. Agglomeration at this length scale gives a gray appearance to

**Table 6. Agglomerate Area Ratio and Transparency of PVDF Nanocomposites Containing 2.0 wt % N-MWNTs**

N-MWNTs	agglomerate area ratio (%)	transparency (%)
synthesis time (0.5 h)	$1.44 \pm 0.48$	53.0
synthesis time (1.0 h)	$1.02 \pm 0.35$	33.1
synthesis time (2.0 h)	$1.8 \pm 0.2$	52
synthesis time (3.0 h)	$1.90 \pm 0.55$	36.3
gas ratio (50:20:80)	$0.76 \pm 0.26$	48.0
gas ratio (50:80:20)	$2.93 \pm 0.81$	60.8
gas ratio (50:50:50)	$1.8 \pm 0.2$	52
gas ratio (70:70:70)	$1.09 \pm 0.71$	44.9

the nanocomposites films and decreases the transparency.<sup>26</sup> The N-MWNTs synthesized at 1.0 h depicted better dispersion at this length scale with a transparency of 33.1% versus 0.5 h (53%), 2.0 h (52%), and 3.0 h (36.3%).

Concerning the effect of gas ratio on the dispersion state, the N-MWNTs synthesized at the ratio of 50:20:80 provided the best dispersion in the PVDF matrix with agglomerate ratio of  $0.76 \pm 0.26\%$  compared to 50:80:20 (i.e.,  $2.93 \pm 0.81\%$ ), 50:50:50 (i.e.,  $1.8 \pm 0.2\%$ ), and 70:70:70 (i.e.,  $1.09 \pm 0.71\%$ ). For 400–700 nm agglomerates, the PVDF nanocomposites containing N-MWNTs synthesized at the gas ratio of 50:80:20 depicted the highest transparency of 60.8%, suggesting poor dispersion of N-MWNTs in visible light length scale, followed by 50:50:50 (i.e., 52%), 50:20:80 (i.e., 48%), and 70:70:70 (i.e., 44.9%). Hence, N-MWNTs synthesized at the gas ratio of 50:20:80 depicted better dispersion at both length scales over 50:80:20, 50:50:50, and 70:70:70. The severe agglomeration of

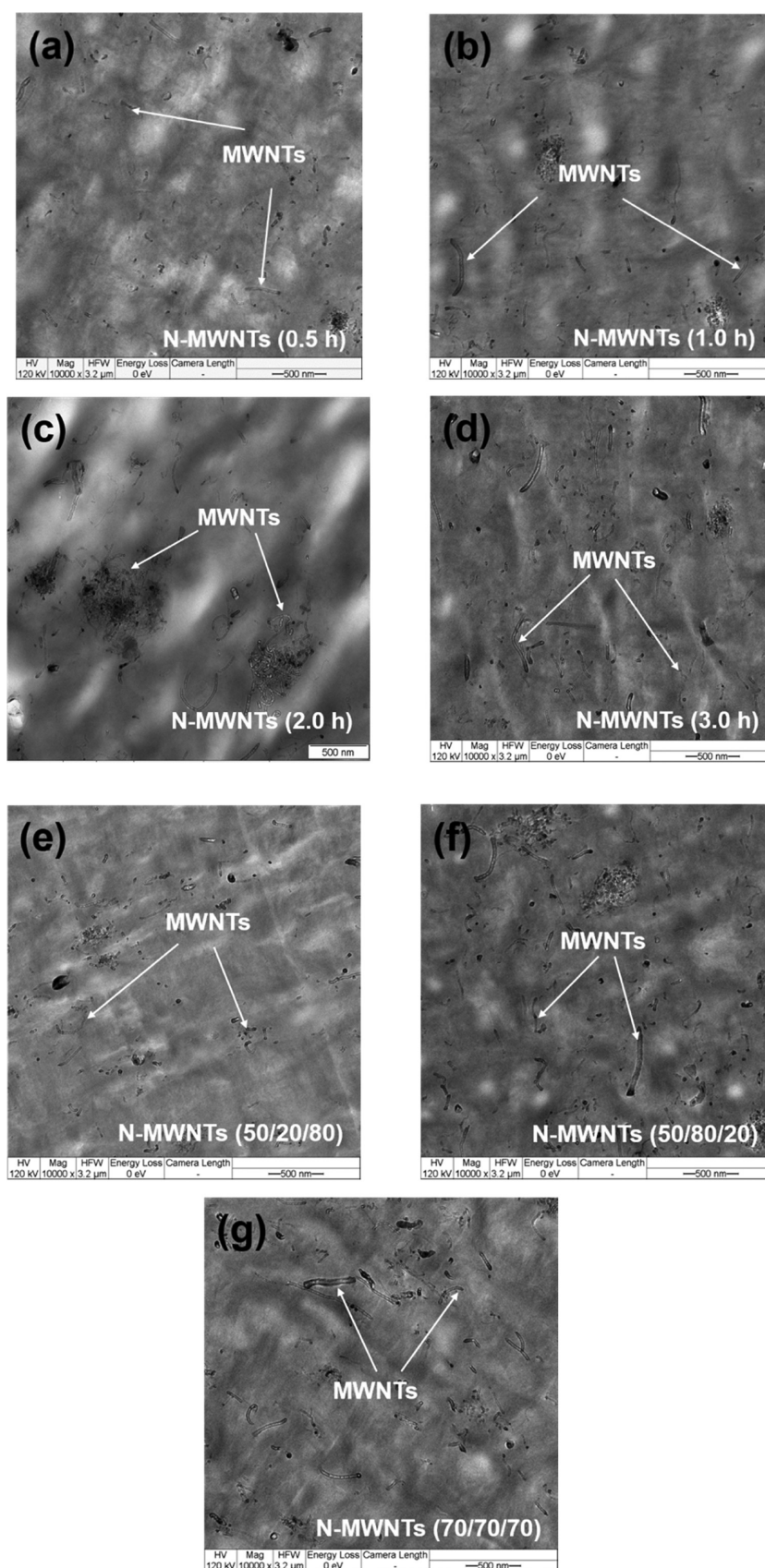


**Figure 5.** TEM micrographs of PVDF nanocomposites containing 2.0 wt% N-MWNTs synthesized at gas ratio of 50:50:50 at different synthesis time (a) 0.5 h, (b) 1.0 h, (c) 2.0 h, and (d) 3.0 h; and at synthesis time of 2.0 h at different gas ratios (e) 50:20:80, (f) 50:80:20, and (g) 70:70:70. TEM micrograph of PVDF nanocomposites containing 2.0 wt % N-MWNTs synthesized at gas ratio of 50:50:50 and 2.0 h synthesis time is presented in (c).

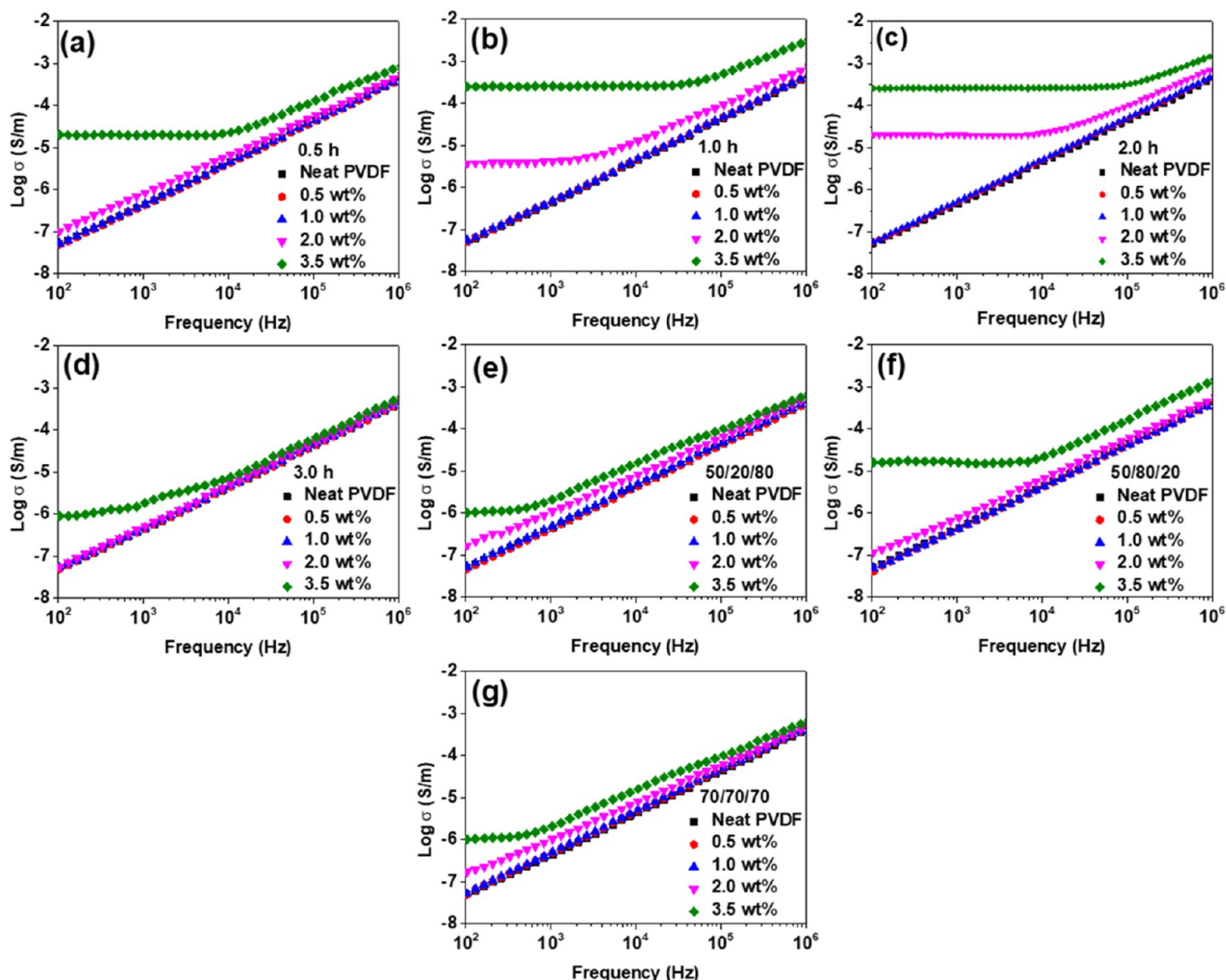


**Figure 6.** Electrical conductivity as a function of frequency for PVDF nanocomposites containing N-MWNTs synthesized at gas ratio of 50:50:50 at different synthesis time (a) 0.5 h, (b) 1.0 h, (c) 2.0 h, and (d) 3.0 h; and at synthesis time of 2.0 h at different gas ratios (e) 50:20:80, (f) 50:80:20, and (g) 70:70:70. Electrical conductivity as a function of frequency for PVDF nanocomposites containing N-MWNTs synthesized at gas ratio of 50:50:50 and 2.0 h synthesis time is presented in (c) (Ameli et al.<sup>13</sup>—(c) is reproduced by permission of Elsevier, Copyright 2013 Elsevier Ltd. All rights reserved).

the N-MWNTs in the PVDF matrix leads to a smaller effective aspect ratio of N-MWNTs, and thus, at a constant loading, deteriorates the ability of the nanotubes to form a network in the PVDF matrix.<sup>33,34</sup>

The nanoscale dispersion of N-MWNTs in the PVDF matrix was assessed using TEM micrographs (Figure 5) of nanocomposites with 2.0 wt % filler. Well-dispersed discrete nanotubes are visible in the TEM micrographs of the PVDF nanocomposites containing all types of N-MWNTs, along with small bundles of N-MWNTs. Only a slight effect of synthesis time on the nanoscale dispersion of N-MWNTs in the PVDF matrix was observed, whereas the gas ratio showed a larger influence. For instance, PVDF nanocomposites containing N-MWNTs synthesized at the gas ratios of 50:80:20 and 50:50:50 showed severe agglomeration of N-MWNTs at microscopic and nanoscopic scales compared to 50:20:80 and 70:70:70.

**2.2.2. Broadband Electrical Conductivity.** Broadband electrical conductivity shows the extent of response or transfer of free charges available in a material when subjected to an external electric field. In general, broadband electrical

conductivity is represented by  $\sigma = \sigma_{DC} + A(\omega)^s$ . Herein,  $\sigma_{DC}$  represents the frequency-independent direct current electrical conductivity, generated due to the movement of charges in phase with the applied electrical field, whereas  $A(\omega)^s$  corresponds to the alternating current (AC) electrical conductivity (i.e.,  $\sigma_{AC}$ ) caused by the out-of-phase movement of charges and is generally frequency-dependent.

Figure 6 shows the electrical conductivity as a function of frequency. The electrical conductivity of neat PVDF depicts an ascending trend with frequency, suggesting that the observed electrical conductivity is mainly due to dipole reorientation. In the case of PVDF nanocomposites, electrical conductivity scales with the amount of N-MWNTs (Figure 6). Depending on the synthesis conditions and structural characteristics, the deviation from the dependence found for PVDF starts at different loadings, illustrating the percolation threshold composition at which the conductive network starts to form. This network formation is greatly influenced by the dispersion quality and aspect ratio of the N-MWNTs, whereas the electrical conductivity of N-MWNTs is governed by structural defects, nitrogen content, and impurities present. For PVDF

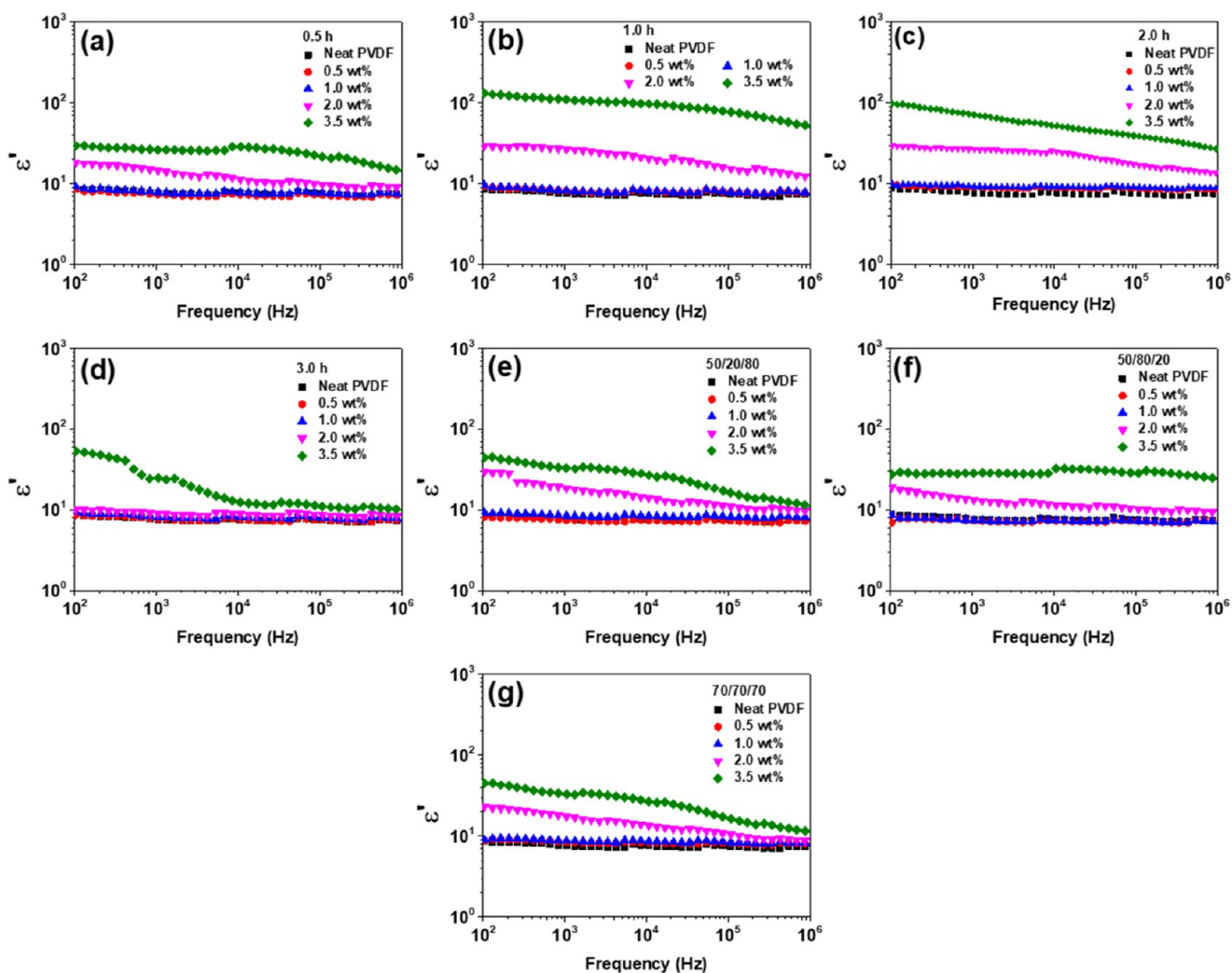


**Figure 7.** Real permittivity as a function of frequency for PVDF nanocomposites containing various amounts of N-MWNTs synthesized at gas ratio of 50:50:50 at different synthesis time (a) 0.5 h, (b) 1.0 h, (c) 2.0 h, and (d) 3.0 h; and at synthesis time of 2.0 h at different gas ratios (e) 50:20:80, (f) 50:80:20, and (g) 70:70:70. Real permittivity as a function of frequency for PVDF nanocomposites containing various amounts of N-MWNTs synthesized at gas ratio of 50:50:50 and 2.0 h synthesis time is presented in (c) (Ameli et al.<sup>13</sup>—(c) is reproduced by permission of Elsevier, Copyright 2013 Elsevier Ltd. All rights reserved).

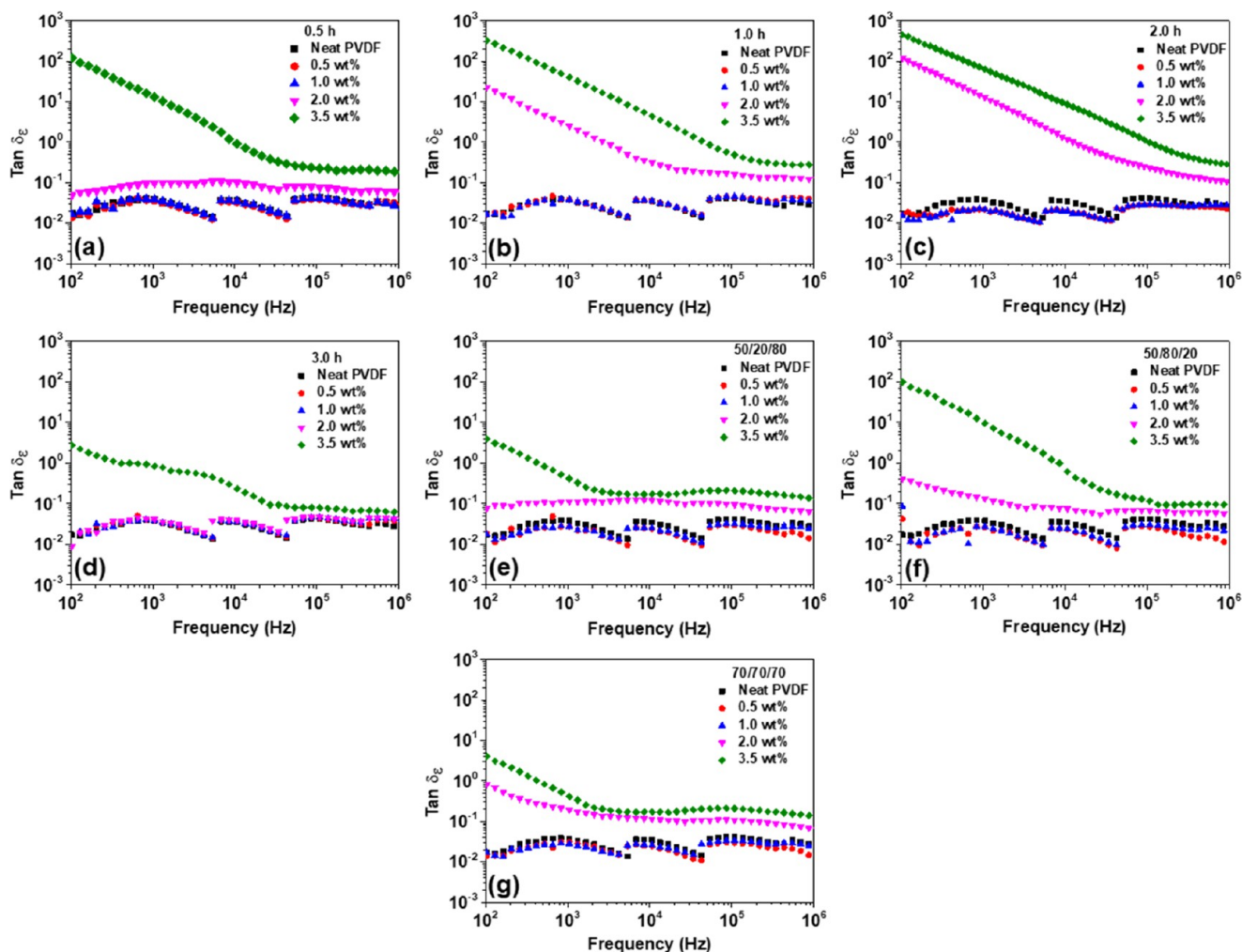
nanocomposites containing N-MWNTs synthesized at 0.5 h, a significant increase in electrical conductivity was observed starting at 3.5 wt % N-MWNTs. At this concentration, the nanocomposite also depicts a semiconducting nature, with a frequency-independent plateau at lower frequencies. This suggests generation of the interconnected networks of N-MWNTs in PVDF matrix, referred as electrical percolation.<sup>35</sup> In case of PVDF nanocomposites containing N-MWNTs synthesized at 1.0 and 2.0 h, electrical percolation was observed at a relatively lower concentration of N-MWNTs, i.e., 2.0 wt %. Moreover, electrical conductivity was significantly higher over 0.5 and 3.0 h at any given amount of N-MWNTs. This illustrates that these samples show an enhanced interconnected network of N-MWNTs, facilitating effective charge transport at small N-MWNT amounts. Therefore, it can be asserted that the synthesis time plays a critical role in designing the electrical conductivity of the nanocomposites. The electrical conductivity results were not in line with the microscopic dispersion (i.e., agglomerate area ratio and relative transparency) as well as the nanoscopic dispersion of N-MWNTs in PVDF matrix.

When varying the gas ratio, electrical percolation was observed at 3.5 wt % for all of the N-MWNTs except N-MWNTs synthesized at a gas ratio of 50:50:50 (Figure 6e–g). For N-MWNTs synthesized at a gas ratio of 50:50:50, a relatively low percolation threshold was observed (i.e., 2 wt %). In this variation, it was observed that the electrical conductivity results were not in line with microscopic dispersion (i.e., agglomerate area ratio) of N-MWNTs in the PVDF matrix. This is due to the fact that the electrical conductivity of PVDF nanocomposites is not only controlled by the state of dispersion of the nanoparticles in the PVDF matrix but also highly influenced by the intrinsic properties of conducting fillers (in this case N-MWNTs), such as inherent electrical conductivity, aspect ratio, amount of defects and nitrogen present, and carbon purity. For instance, at 3.5 wt %, enhanced electrical conductivity was found for the N-MWNTs synthesized at the gas ratio of 50:50:50, having relatively high carbon purity, high aspect ratio, and optimum powder electrical conductivity.

**2.2.3. Broadband Dielectric Permittivity.** To study the charge-storage properties, real ( $\epsilon'$ ) and imaginary ( $\epsilon''$ ) parts of

**Table 7.** Real Permittivity ( $\epsilon'$ ) and Dissipation Factor ( $\tan \delta_e$ ) of PVDF Nanocomposites Containing N-MWNTs with Various Concentrations of N-MWNTs at 1 kHz

type of N-MWNT	PVDF/0.5 wt % N-MWNT		PVDF/1.0 wt % N-MWNT		PVDF/2.0 wt % N-MWNT		PVDF/3.5 wt % N-MWNT	
	$\epsilon'$	$\tan \delta_e$	$\epsilon'$	$\tan \delta_e$	$\epsilon'$	$\tan \delta_e$	$\epsilon'$	$\tan \delta_e$
synthesis time (0.5 h)	7.4	0.03	7.88	0.03	14.5	0.09	26.39	12.93
synthesis time (1.0 h)	8.16	0.03	8.23	0.03	26.76	2.49	109.7	39.95
synthesis time (2.0 h)	8.9	0.02	9.3	0.02	26.8	12.7	71.26	63.2
synthesis time (3.0 h)	7.72	0.03	8.2	0.03	8.94	0.04	24.77	0.83
gas ratio (50:20:80)	7.48	0.02	8.46	0.02	18.6	0.11	32.8	0.41
gas ratio (50:80:20)	7.32	0.02	7.43	0.02	13.26	0.13	28.4	9.5
gas ratio (50:50:50)	8.9	0.02	9.3	0.02	26.8	12.7	71.26	63.2
gas ratio (70:70:70)	8.43	0.03	8.75	0.02	17.38	0.19	32.8	0.41

**Figure 8.** Dissipation factor ( $\tan \delta_e$ ) as a function of frequency for PVDF nanocomposites containing various amounts of N-MWNTs synthesized at gas ratio of 50:50:50 at different synthesis time (a) 0.5 h, (b) 1.0 h, (c) 2.0 h, and (d) 3.0 h; and at synthesis time of 2.0 h at different gas ratios (e) 50:20:80, (f) 50:80:20, and (g) 70:70:70.  $\tan \delta_e$  as a function of frequency for PVDF nanocomposites containing various amounts of N-MWNTs synthesized at gas ratio of 50:50:50 and 2.0 h synthesis time is presented in (c).

the complex permittivity ( $\epsilon = \epsilon' + i\epsilon''$ ) of neat PVDF and PVDF nanocomposites were assessed. The real part of permittivity ( $\epsilon'$ ) represents the charge-storage ability of the material, which is directly related to the polarization inside the material. The imaginary part of permittivity corresponds to the loss of energy in the material. In the case of charge-storing materials, the materials should possess high real permittivity alongside with ultralow imaginary permittivity. In this context,

the dissipation factor ( $\tan \delta_e = \epsilon''/\epsilon'$ ) is an effective measure for the charge-storing ability of materials.

Figure 7 shows the real permittivity as a function of frequency for neat PVDF and PVDF nanocomposites containing various amounts of N-MWNTs, and values at 1 kHz are summarized in Table 7 together with the values of  $\tan \delta_e$ . In the case of PVDF/N-MWNT nanocomposites, due to significant differences in the conductivity of the matrix (i.e., PVDF) and the filler (i.e., N-MWNTs), the interfacial

polarization is overwhelming. In this case, nomadic charges get accumulated at the interfaces, leading to charge polarization. Since interfacial polarization occurs at a large relaxation time, this phenomenon is predominant at lower frequencies and becomes negligible at higher frequencies. This is well evident from the frequency-dependent analysis of the dielectric permittivity of the PVDF nanocomposites (Figure 7). In the case of PVDF nanocomposites, real permittivity scales with the amount of N-MWNTs, whereby again, depending on synthesis conditions, different amounts of nanotubes are needed to show a deviation from the curve found for pure PVDF. It is well established that the formation of nanocapacitors (adjacent conducting N-MWNTs surrounded by thin insulating layer of the polymer matrix) in a multiphase system, such as conductive polymer nanocomposites, greatly controls the interfacial polarization as well as the electronic polarization.<sup>36</sup> Therefore, with increasing the amount of N-MWNTs in the PVDF nanocomposites, the distance between discrete N-MWNTs decreases, leading to the generation of nanocapacitors. This further results in enhanced capacitance in the materials as well as real permittivity.

In case of the PVDF nanocomposites containing N-MWNTs,  $\epsilon'$  is in line with the observed electrical conductivity of the nanocomposites and scales with the amount of N-MWNTs. Thereby, better connected networks of N-MWNTs, facilitated by proper dispersion of higher aspect ratio N-MWNTs, combined with higher carbon purity in the PVDF matrix resulted in larger values of  $\epsilon'$ . Moreover, apart from interfacial polarization in nanocomposites, self-polarization in N-MWNTs, arising from the presence of nitrogen and structural defects, also led to enhanced  $\epsilon'$ . However,  $\epsilon'$  was not in line with the amount of nitrogen and defects present. This was due to the overwhelming effect of electrical conductivity, arising from the interconnected network of conducting N-MWNTs on  $\epsilon'$ .

For instance, owing to well-connected network of efficiently dispersed N-MWNTs (i.e., high electrical conductivity) as well as a higher amount of self-polarization, the PVDF nanocomposites containing 3.5 wt % N-MWNTs synthesized at 1.0 h depicted the highest  $\epsilon'$  of 109.7 over 0.5, 2.0, and 3.0 h at 1 kHz (Table 7). The tuned functional properties of N-MWNTs by varying gas ratios depicted noteworthy effect on  $\epsilon'$  of PVDF nanocomposites, where significantly enhanced  $\epsilon'$  in the case of N-MWCNTs synthesized at the gas ratio of 50:50:50 was due to relatively higher electrical conductivity (i.e., better interconnected networks) and a higher amount of nitrogen content (i.e., self-polarization).

**2.2.4. Broadband Dissipation Factor ( $\tan \delta_e$ ).** The broadband dissipation factor ( $\tan \delta_e$ ) is an essential parameter for charge-storage applications and determines the energy loss in materials. For best charge-storage application, materials should possess minimum  $\tan \delta_e$ . The  $\tan \delta_e$  is mainly related to the Ohmic loss, arising from the nomadic charge transfer in the materials. Therefore, large  $\tan \delta_e$  in conducting materials is obvious. In case of conductive polymer nanocomposites, interconnected networks of conducting nanoparticles provide pathways for nomadic charges to move in the material, leading to dissipation of energy and thus a large value of  $\tan \delta_e$ .

When an AC field is applied, as frequency decreases, the time available for the transfer of nomadic charges is higher; therefore, a higher amount of energy gets dissipated. This further results in increased  $\tan \delta_e$  of the materials with decreasing frequency. Figure 8a–d shows  $\tan \delta_e$  as a function

of frequency for PVDF nanocomposites containing various amounts of N-MWNTs synthesized at different times. The  $\tan \delta_e$  of PVDF nanocomposites is well in line with the electrical conductivity of the nanocomposites and is observed to increase with increasing the amount of N-MWNTs in the PVDF matrix.

Above the percolation threshold,  $\tan \delta_e$  considerably increased at lower frequencies, where the time for nomadic charge transfer was higher. As observed earlier, the highest amount of nitrogen present (i.e., polarizing centers), highest carbon purity, and largest inherent electrical conductivity of N-MWNTs resulted in high  $\epsilon'$ . In contrast, a large amount of nitrogen and defect sites, low aspect ratio, and poor dispersion in the PVDF matrix led to the lack of or less developed interconnected network of N-MWNTs, resulting in restricted movement of nomadic charges, and thus smaller  $\tan \delta_e$ . For instance, in the case of PVDF nanocomposites containing 3.5 wt % N-MWNTs synthesized at 3.0 h, at 1 kHz, significantly higher  $\epsilon'$  of 24.8 alongside a very small dissipation factor (i.e.,  $\tan \delta_e = \frac{\epsilon''}{\epsilon'}$ ) of 0.83 was observed (Table 7). This confirms enhanced charge-storage ability of the fabricated nanocomposites.

In case of the PVDF nanocomposites containing N-MWNTs synthesized at different gas ratios,  $\tan \delta_e$  was observed to be in line with the electrical conductivity of the nanocomposites (Figure 8e–g). Herein, high carbon purity, large inherent electrical conductivity, and less amount of nitrogen, i.e., less scattering centers for nomadic charges, led to the highest current leakage through N-MWNTs networks and thus largest  $\tan \delta_e$ . On the other hand, Table 7 shows PVDF nanocomposites containing 3.5 wt % N-MWNTs synthesized at the gas ratios of 50:20:80 and 70:70:70 depicted a dissipation factor of 0.41 along with significantly higher  $\epsilon'$  of 32.8 over neat PVDF (i.e., 7.7) at 1 kHz. This originates from the higher amount of nitrogen present in N-MWNTs and better dispersion, which results in higher  $\epsilon'$  through self-polarization and interfacial polarization. The low  $\tan \delta_e$  was realized through a suitable balance between resistances offered by nitrogen against nomadic charge transfer. This suggests that larger nomadic charges can be stored in polymer-based nanocomposites (in this case PVDF) by effectively dispersing nitrogen-doped CNTs with a specific set of properties, which can be tuned by tailoring the synthesis parameters, such as time and gas ratio.

### 3. CONCLUSIONS

In this study, the effect of N-MWNTs structure on the broadband dielectric properties of N-MWNTs/PVDF nanocomposites was systematically investigated. N-MWNTs with different structures and nitrogen contents were synthesized by varying the feed gas ratio and the synthesis time. Nitrogen doping was employed to generate charge polarizing centers within the MWNTs, which facilitate large nomadic charge storage. It was observed that various parameters, such as carbon purity, nitrogen content, defect amount, aspect ratio, and inherent electrical conductivity of N-MWNTs alongside their nanoscopic and microscopic dispersion in PVDF, control the dielectric properties of the final nanocomposites. The less defective N-MWNTs showed higher thermal stability, whereas a larger amount of carbon precursor resulted in higher carbon purity. Higher crystallinity in N-MWNTs correlated with the growth of longer N-MWNTs, which resulted in better

interconnected network of N-MWNTs in PVDF (i.e., there was a higher conductivity at a given loading above percolation). The inherent electrical conductivity of N-MWNTs scaled with the carbon purity. It was expected that the final electrical conductivity scales with the inherent conductivity of N-MWNTs; however, in this study, it was strongly influenced by the dispersion quality and aspect ratio of the N-MWNTs. Finally, enhanced charge storage in N-MWNT/PVDF nanocomposites was achieved by the higher amount of nitrogen heteroatoms (i.e., large self-polarization), high carbon purity, and better dispersion quality of N-MWNTs in PVDF matrix. Finally, in the PVDF-based nanocomposites, the best combinations of high values of the real part of complex permittivity ( $\epsilon'$ ) and lowest  $\tan \delta_e$  were achieved for N-MWNTs synthesized at the gas ratios of argon/ethane/nitrogen 50:20:80 and 70:70:70 at 2.0 h, followed by those synthesized at the gas ratio of 50:50:50 for 3.0 h.

## 4. EXPERIMENTAL SECTION

**4.1. Materials.** A semicrystalline PVDF polymer (11008/0001) with a melting point of 160 °C and an average density of 1.78 g/cm<sup>3</sup> was procured from 3M Canada. N-MWNTs were grown on Fe catalyst using chemical vapor deposition (CVD) technique, described in a previous work.<sup>11</sup> To study the effect of synthesis time, N-MWNTs were synthesized at four different synthesis time (i.e., 0.5, 1.0, 2.0, and 3.0 h) at 750 °C with an argon/ethane/nitrogen mixture of 50:50:50 sccm. Since precursors' gas ratio greatly controls the carbon purity and also influences the amount of nitrogen present (i.e., number of polarizing centers), to study its effect on structural and electrical properties of N-MWNTs, a set of N-MWNTs was synthesized at different gas feed (argon/ethane/nitrogen) ratios of 50:80:20, 50:20:80, 50:50:50, and 70:70:70 sccm at 750 °C for 2.0 h. For a complete understanding of the effects of synthesis time and gas ratio, the results of N-MWNTs prepared with synthesis time of 2.0 h and gas ratio of 50:50:50 have been taken from a previous study<sup>13</sup> and compared with the results obtained in this study.

**4.2. Nanocomposite Preparation.** The PVDF nanocomposites containing various contents of N-MWNTs were prepared using an Alberta polymer asymmetric minimixer (APAM) at 240 °C and a rotor speed of 235 rpm. In a typical process, PVDF granules were masticated for 3 min at 240 °C. Thereafter, desired amounts of N-MWNTs were inserted into the APAM cup, and mixing was continued for an extra 14 min. The PVDF nanocomposites were prepared with various concentrations of N-MWNTs (i.e., 0.5, 1.0, 2.0, and 3.5 wt %). A Carver compression molder (Carver Inc., Wabash, IN) was used to prepare circular samples for further characterizations.

**4.3. N-MWNTs Characterization.** The morphology and average size distribution of the synthesized N-MWNTs were assessed using transmission electron microscopy (TEM). The TEM micrographs of N-MWNTs were captured using a Libra 200 (Carl Zeiss GmbH, Germany) TEM microscope. The quantitative analysis of the length distribution was performed by estimating the distribution parameters of  $x_{10}$ ,  $x_{50}$ , and  $x_{90}$ , indicating that 10, 50, and 90% of N-MWNTs are smaller in length than that of the specified value, respectively. To study the general structure of the produced nanotube material, scanning electron micrographs of N-MWNTs were captured using an Ultra 55 SEM from Zeiss at an accelerating voltage of 3 kV.

The quantitative analysis of the amount of nitrogen present in N-MWNTs was performed using an X-ray photoelectron spectrometer (AXIS ULTRA from Kratos Analytical, England). The structural properties of individual N-MWNTs were assessed using Raman imaging system WITEC Alpha 300R with a 532 nm laser. The thermal stability of synthesized N-MWNTs was assessed using a thermogravimetric analyzer (TA Instruments: TGA Q500). The experiments were performed under air atmosphere in the temperature range of 25–800 °C at a heating rate of 10 °C/min. The powder electrical conductivity of N-MWNTs was analyzed using PuLeMe Pulverleitfähigkeitsmessung instrument. The electrical conductivity was recorded as a function of the applied pressure. Further information can be found in previous studies.<sup>37,38</sup>

**4.4. PVDF Nanocomposite Characterization.** The dispersion of N-MWNTs in the PVDF matrix was assessed at three different length scales. The microdispersion state of N-MWNTs was studied using light transmission microscopy on 5  $\mu$ m thin film cuts from the compression molded samples using a Leica microtome RM2265 (Leica Microsystems GmbH, Wetzlar, Germany). The Stream Motion (Olympus) software was used to analyze the agglomerate area ratio in percentage ( $A_A\%$ ). Another evidence of microdispersion state of N-MWNTs in the PVDF matrix was recorded from the relative transparency of the background of thin cuts. The relative transparency reflects the amount of agglomerates with the size equal to or greater than the wavelength of the visible light (i.e., 400–700 nm), but smaller than agglomerates visually observable in the micrographs. The nanodispersion state of N-MWNTs in the PVDF matrix was assessed using TEM micrographs. For TEM imaging, 60 nm thin films were cut from the compression molded samples using an ultramicrotome EM UC6. TEM micrographs of the PVDF nanocomposites were captured using a Libra 200 (Carl Zeiss GmbH, Germany) TEM microscope. Further information can be found in previous studies.<sup>26,39</sup>

The broadband dielectric properties of PVDF nanocomposites containing N-MWNTs were assessed using a Bio-Logic impedance analyzer (SP-200 EIS) in the frequency range of 10<sup>2</sup>–10<sup>7</sup> Hz. At least three different samples were measured for each set of the PVDF nanocomposites. For the measurement purpose, a Solartron 12962 sample holder with an electrode diameter of 10 mm was connected to a Bio-Logic impedance analyzer. All of the measurements were performed at an applied voltage of 100 mV.

## ■ ASSOCIATED CONTENT

### 📄 Supporting Information

The Supporting Information is available free of charge on the ACS Publications website at DOI: [10.1021/acsomega.8b01239](https://doi.org/10.1021/acsomega.8b01239).

XPS and Raman spectra for N-MWNTs synthesized at different synthesis time and gas ratios (PDF)

## ■ AUTHOR INFORMATION

### Corresponding Authors

\*E-mail: [sbose@iisc.ac.in](mailto:sbose@iisc.ac.in) (S.B.).

\*E-mail: [u.sundararaj@ucalgary.ca](mailto:u.sundararaj@ucalgary.ca) (U.S.).

### ORCID

Mohammad Arjmand: 0000-0002-8812-5638

Petra Pötschke: 0000-0001-6392-7880

Suryasarathi Bose: 0000-0001-8043-9192

Uttandaraman Sundararaj: 0000-0003-4124-3917

### Author Contributions

<sup>†</sup>S.P.P. and M.A. made equal contribution to this work.

### Notes

The authors declare no competing financial interest.

## ACKNOWLEDGMENTS

The authors thank Manuela Heber (IPF Dresden) for TEM micrographs of N-MWNTs and PVDF/N-MWNT nanocomposites and Frank Simon for XPS measurements. S.P.P. thanks the DST-DAAD (ID 57213508) for supporting the travel and a stay at IPF Dresden. The authors are grateful to Samaneh Dordani Haghighi for designing and drawing the graphical abstract.

## REFERENCES

- (1) Dang, Z.-M.; Wu, J.-P.; Xu, H.-P.; Yao, S.-H.; Jiang, M.-J.; Bai, J. Dielectric Properties of Upright Carbon Fiber Filled Poly (Vinylidene Fluoride) Composite with Low Percolation Threshold and Weak Temperature Dependence. *Appl. Phys. Lett.* **2007**, *91*, No. 072912.
- (2) He, F.; Lau, S.; Chan, H. L.; Fan, J. High Dielectric Permittivity and Low Percolation Threshold in Nanocomposites Based on Poly (Vinylidene Fluoride) and Exfoliated Graphite Nanoplates. *Adv. Mater.* **2009**, *21*, 710–715.
- (3) Kim, J. Y.; Lee, W. H.; Suk, J. W.; Potts, J. R.; Chou, H.; Kholmanov, I. N.; Piner, R. D.; Lee, J.; Akinwande, D.; Ruoff, R. S. Chlorination of Reduced Graphene Oxide Enhances the Dielectric Constant of Reduced Graphene Oxide/Polymer Composites. *Adv. Mater.* **2013**, *25*, 2308–2313.
- (4) Dang, Z.-M.; Fan, L.-Z.; Shen, Y.; Nan, C.-W. Dielectric Behavior of Novel Three-Phase MWNTs/BaTiO<sub>3</sub>/PVDF Composites. *Mater. Sci. Eng., B* **2003**, *103*, 140–144.
- (5) Pawar, S. P.; Arjmand, M.; Gandhi, M.; Bose, S.; Sundararaj, U. Critical Insights into Understanding the Effects of Synthesis Temperature and Nitrogen Doping Towards Charge Storage Capability and Microwave Shielding in Nitrogen-Doped Carbon Nanotube/Polymer Nanocomposites. *RSC Adv.* **2016**, *6*, 63224–63234.
- (6) Dimiev, A.; Lu, W.; Zeller, K.; Crowgey, B.; Kempel, L. C.; Tour, J. M. Low-Loss, High-Permittivity Composites Made from Graphene Nanoribbons. *ACS Appl. Mater. Interfaces* **2011**, *3*, 4657–4661.
- (7) Yang, C.; Lin, Y.; Nan, C. Modified Carbon Nanotube Composites with High Dielectric Constant, Low Dielectric Loss and Large Energy Density. *Carbon* **2009**, *47*, 1096–1101.
- (8) Li, Q.; Xue, Q.; Zheng, Q.; Hao, L.; Gao, X. Large Dielectric Constant of the Chemically Purified Carbon Nanotube/Polymer Composites. *Mater. Lett.* **2008**, *62*, 4229–4231.
- (9) Wu, C.; Huang, X.; Wu, X.; Xie, L.; Yang, K.; Jiang, P. Graphene Oxide-Encapsulated Carbon Nanotube Hybrids for High Dielectric Performance Nanocomposites with Enhanced Energy Storage Density. *Nanoscale* **2013**, *5*, 3847–3855.
- (10) Arjmand, M.; Ameli, A.; Sundararaj, U. Employing Nitrogen Doping as Innovative Technique to Improve Broadband Dielectric Properties of Carbon Nanotube/Polymer Nanocomposites. *Macromol. Mater. Eng.* **2016**, *301*, 555–565.
- (11) Arjmand, M.; Chizari, K.; Krause, B.; Poetschke, P.; Sundararaj, U. Effect of Synthesis Catalyst on Structure of Nitrogen-Doped Carbon Nanotubes and Electrical Conductivity and Electromagnetic Interference Shielding of Their Polymeric Nanocomposites. *Carbon* **2016**, *98*, 358–372.
- (12) Watts, P. C.; Hsu, W. K.; Barnes, A.; Chambers, B. High Permittivity from Defective Multiwalled Carbon Nanotubes in the X-Band. *Adv. Mater.* **2003**, *15*, 600–603.
- (13) Ameli, A.; Arjmand, M.; Pötschke, P.; Krause, B.; Sundararaj, U. Effects of Synthesis Catalyst and Temperature on Broadband Dielectric Properties of Nitrogen-Doped Carbon Nanotube/Polyvinylidene Fluoride Nanocomposites. *Carbon* **2016**, *106*, 260–278.
- (14) Li, J.; Ma, P. C.; Chow, W. S.; To, C. K.; Tang, B. Z.; Kim, J. K. Correlations between Percolation Threshold, Dispersion State, and Aspect Ratio of Carbon Nanotubes. *Adv. Funct. Mater.* **2007**, *17*, 3207–3215.
- (15) Ayatollahi, M.; Shadlou, S.; Shokrieh, M.; Chitsazzadeh, M. Effect of Multi-Walled Carbon Nanotube Aspect Ratio on Mechanical and Electrical Properties of Epoxy-Based Nanocomposites. *Polym. Test.* **2011**, *30*, 548–556.
- (16) Jang, J. W.; Lee, C. E.; Lyu, S. C.; Lee, T. J.; Lee, C. J. Structural Study of Nitrogen-Doping Effects in Bamboo-Shaped Multiwalled Carbon Nanotubes. *Appl. Phys. Lett.* **2004**, *84*, 2877–2879.
- (17) Panchakarla, L.; Govindaraj, A.; Rao, C. Boron- and Nitrogen-Doped Carbon Nanotubes and Graphene. *Inorg. Chim. Acta* **2010**, *363*, 4163–4174.
- (18) Chouit, F.; Guellati, O.; Boukhezar, S.; Harat, A.; Guerioune, M.; Badi, N. Synthesis and Characterization of HDPE/N-MWNT Nanocomposite Films. *Nanoscale Res. Lett.* **2014**, *9*, No. 288.
- (19) Fujisawa, K.; Tojo, T.; Muramatsu, H.; Elías, A. L.; Vega-Díaz, S. M.; Tristán-López, F.; Kim, J. H.; Hayashi, T.; Kim, Y. A.; Endo, M.; Terrones, M. Enhanced Electrical Conductivities of N-Doped Carbon Nanotubes by Controlled Heat Treatment. *Nanoscale* **2011**, *3*, 4359–4364.
- (20) Kanygin, M.; Sedelnikova, O.; Asanov, I.; Bulusheva, L.; Okotrub, A.; Kuzhir, P.; Plyushch, A.; Maksimenko, S.; Lapko, K.; Sokol, A.; et al. Effect of Nitrogen Doping on the Electromagnetic Properties of Carbon Nanotube-Based Composites. *J. Appl. Phys.* **2013**, *113*, No. 144315.
- (21) Glerup, M.; Castignolles, M.; Holzinger, M.; Hug, G.; Loiseau, A.; Bernier, P. Synthesis of Highly Nitrogen-Doped Multi-Walled Carbon Nanotubes. *Chem. Commun.* **2003**, 2542–2543.
- (22) Choi, H. C.; Park, J.; Kim, B. Distribution and Structure of N Atoms in Multiwalled Carbon Nanotubes Using Variable-Energy X-Ray Photoelectron Spectroscopy. *J. Phys. Chem. B* **2005**, *109*, 4333–4340.
- (23) Arjmand, M.; Sundararaj, U. Effects of Nitrogen Doping on X-Band Dielectric Properties of Carbon Nanotube/Polymer Nanocomposites. *ACS Appl. Mater. Interfaces* **2015**, *7*, 17844–17850.
- (24) Krause, B.; Ritschel, M.; Täschner, C.; Oswald, S.; Gruner, W.; Leonhardt, A.; Pötschke, P. Comparison of Nanotubes Produced by Fixed Bed and Aerosol-CVD Methods and Their Electrical Percolation Behaviour in Melt Mixed Polyamide 6.6 Composites. *Compos. Sci. Technol.* **2010**, *70*, 151–160.
- (25) Sumpter, B. G.; Meunier, V.; Romo-Herrera, J. M.; Cruz-Silva, E.; Cullen, D. A.; Terrones, H.; Smith, D. J.; Terrones, M. Nitrogen-Mediated Carbon Nanotube Growth: Diameter Reduction, Metallicity, Bundle Dispersability, and Bamboo-Like Structure Formation. *ACS Nano* **2007**, *1*, 369–375.
- (26) Arjmand, M.; Sundararaj, U. Electromagnetic Interference Shielding of Nitrogen-Doped and Undoped Carbon Nanotube/Polyvinylidene Fluoride Nanocomposites: A Comparative Study. *Compos. Sci. Technol.* **2015**, *118*, 257–263.
- (27) Sharifi, T.; Nitze, F.; Barzegar, H. R.; Tai, C.-W.; Mazurkiewicz, M.; Malolepszy, A.; Stobinski, L.; Wägberg, T. Nitrogen Doped Multi Walled Carbon Nanotubes Produced by CVD-Correlating XPS and Raman Spectroscopy for the Study of Nitrogen Inclusion. *Carbon* **2012**, *50*, 3535–3541.
- (28) Ayala, P.; Arenal, R.; Rummeli, M.; Rubio, A.; Pichler, T. The Doping of Carbon Nanotubes with Nitrogen and Their Potential Applications. *Carbon* **2010**, *48*, 575–586.
- (29) Shin, W. H.; Jeong, H. M.; Kim, B. G.; Kang, J. K.; Choi, J. W. Nitrogen-Doped Multiwall Carbon Nanotubes for Lithium Storage with Extremely High Capacity. *Nano Lett.* **2012**, *12*, 2283–2288.
- (30) Lyu, S.; Kim, H.; Kim, S.; Park, J.; Lee, C. Synthesis and Crystallinity of Carbon Nanotubes Produced by a Vapor-Phase Growth Method. *Appl. Phys. A* **2004**, *79*, 697–700.
- (31) Ma, P.-C.; Siddiqui, N. A.; Marom, G.; Kim, J.-K. Dispersion and Functionalization of Carbon Nanotubes for Polymer-Based Nanocomposites: A Review. *Composites, Part A* **2010**, *41*, 1345–1367.

(32) Song, Y. S.; Youn, J. R. Influence of Dispersion States of Carbon Nanotubes on Physical Properties of Epoxy Nanocomposites. *Carbon* **2005**, *43*, 1378–1385.

(33) Bose, S.; Bhattacharyya, A. R.; Bondre, A. P.; Kulkarni, A. R.; Pötschke, P. Rheology, Electrical Conductivity, and the Phase Behavior of Cocontinuous PA6/ABS Blends with MWNT: Correlating the Aspect Ratio of MWNT with the Percolation Threshold. *J. Polym. Sci., Part B: Polym. Phys.* **2008**, *46*, 1619–1631.

(34) Guo, J.; Liu, Y.; Prada-Silvy, R.; Tan, Y.; Azad, S.; Krause, B.; Pötschke, P.; Grady, B. P. Aspect Ratio Effects of Multi-Walled Carbon Nanotubes on Electrical, Mechanical, and Thermal Properties of Polycarbonate/MWCNT Composites. *J. Polym. Sci., Part B: Polym. Phys.* **2014**, *52*, 73–83.

(35) Bauhofer, W.; Kovacs, J. Z. A Review and Analysis of Electrical Percolation in Carbon Nanotube Polymer Composites. *Compos. Sci. Technol.* **2009**, *69*, 1486–1498.

(36) Dang, Z.-M.; Yao, S.-H.; Yuan, J.-K.; Bai, J. Tailored Dielectric Properties Based on Microstructure Change in BaTiO<sub>3</sub>-Carbon Nanotube/Polyvinylidene Fluoride Three-Phase Nanocomposites. *J. Phys. Chem. C* **2010**, *114*, 13204–13209.

(37) Krause, B.; Pötschke, P.; Ilin, E.; Predtechenskiy, M. Melt Mixed SWCNT-Polypropylene Composites with Very Low Electrical Percolation. *Polymer* **2016**, *98*, 45–50.

(38) Krause, B.; Boldt, R.; Häußler, L.; Pötschke, P. Ultralow Percolation Threshold in Polyamide 6.6/MWCNT Composites. *Compos. Sci. Technol.* **2015**, *114*, 119–125.

(39) Pawar, S. P.; Gandhi, M.; Arief, I.; Krause, B.; Pötschke, P.; Bose, S. Graphene Derivatives Doped with Nickel Ferrite Nanoparticles as Excellent Microwave Absorbers in Soft Nanocomposites. *ChemistrySelect* **2017**, *2*, 5984–5999.